



Kinetic study of the photo-Fenton degradation of formic acid Combined effects of temperature and iron concentration

Jorgelina Farias^a, Enrique D. Albizzati^b, Orlando M. Alfano^{a,*}

^a Instituto de Desarrollo Tecnológico para la Industria Química (INTEC), Consejo Nacional de Investigaciones Científicas y Técnicas (CONICET) and Universidad Nacional del Litoral (UNL), Güemes 3450, 3000 Santa Fe, Argentina

^b Facultad de Ingeniería Química, Universidad Nacional del Litoral (UNL), Santiago del Estero 2654, 3000 Santa Fe, Argentina

ARTICLE INFO

Article history:

Available online 8 February 2009

Keywords:

Photo-Fenton reaction
Temperature effect
Iron concentration effect
D-optimal design
Arrhenius parameters
Formic acid

ABSTRACT

This study is focused on the kinetic modelling of the Fenton and photo-Fenton degradation of a model pollutant (formic acid) in aqueous solution, for relatively low iron concentrations (1–9 ppm). The reaction rate expressions are derived from an accepted reaction mechanism and explicitly having into account the local volumetric rate of photon absorption. The experimental work was performed in a well-stirred tank laboratory reactor irradiated from the bottom. Afterward, the proposed kinetic model and the experimental data were used to estimate the Arrhenius parameters between 20 and 55 °C, applying a non-linear regression procedure. To avoid the precipitation of iron compounds during the experimental runs, simultaneous high reaction temperatures (55 °C) and iron concentrations (9 ppm) were prevented. To achieve this goal, an experimental design based on the D-optimality criterion was adopted. The proposed kinetic model was able to reproduce the combined effects of changing the ferric iron concentrations, reaction temperatures, and formic acid to hydrogen peroxide molar ratios on the pollutant degradation rate. Kinetic model predictions are compared with experimental data of the organic compound conversion, and a good agreement is obtained. For the whole set of Fenton and photo-Fenton experimental runs, the maximum root mean square error is 7.64%.

© 2009 Elsevier B.V. All rights reserved.

1. Introduction

Fenton reaction is known by its capacity for oxidizing and mineralizing a great variety of toxic and non-biodegradable compounds. It is also known that the Fenton degradation rate can be considerably increased by irradiating the solution with UV or UV/vis radiation [1–6]. Moreover, feasibility of applying solar radiation as a source of UV/vis radiation has made the photo-Fenton system an economical and competitive process [7,8].

The capacities of the Fenton and photo-Fenton systems to destroy these recalcitrant organic pollutants are modified by some operating parameters, such as the hydrogen peroxide and iron concentrations, and the reaction temperature. It has been shown that an increase of the reacting medium temperature of the Fenton mixture can improve the efficiency of the pollutant degradation. Several attempts have been made to investigate the temperature effects on the mineralization of aqueous organic compounds, using artificial [9–11] or solar [12–15] radiation. Also, based on the use of the entire spectrum of the sun, an interesting combined photo-chemical-thermal solar radiation process has been proposed to

study the influence of temperature and solar radiation on a pollutant degradation rate by using the Fenton and photo-Fenton processes [16].

As mentioned above, the iron concentration is another important operating variable that may increase the degradation rate of the Fenton process. Relatively high amounts of iron, equal to or higher than 56 ppm (1 mM), have been used to study the mineralization of various aqueous organic compounds: 2,4-dichlorophenoxyacetic acid (2,4-D) [17] and 2,4,5-trichlorophenoxyacetic acid (2,4,5-T) [18], chlorinated compounds of cellulose bleaching effluents [12], formic acid [19,15], and 2-chlorophenol [20]. On the contrary, it has been demonstrated that low iron concentrations (for example, lower than 20 ppm) are high enough to degrade several toxic pollutants dissolved in water: 4-nitrophenol (4-NP) [16], alachlor [14], EU priority hazardous substances [21], and textile reactive dyes [22]. Due to the possibility of using a photo-Fenton process as a pre-treatment of a conventional biological treatment, some of these contributions were aimed to identify the highest amount of iron compatible with the subsequent biological process without decreasing the process efficiency. Likewise, this low amount of iron is useful for avoiding the subsequent separation step by ferric hydroxide precipitation at the end of the chemical oxidation [21,22]. However, it is worth noting that simultaneous reaction temperatures of about 55 °C and

* Corresponding author. Tel.: +54 342 4511546; fax: +54 342 4511087.
E-mail address: alfano@intec.unl.edu.ar (O.M. Alfano).

Nomenclature

<i>A</i>	reparameterized parameter
<i>B</i>	reparameterized parameter
<i>C</i>	molar concentration (M)
<i>E</i>	activation energy (kJ mol ⁻¹)
e_{λ}^a	spectral local volumetric rate of photon absorption (LVRPA), (Einstein cm ⁻⁴ s ⁻¹)
<i>f</i>	normalized spectral distribution of the lamp output power
<i>k</i>	kinetic constant (M ⁻¹ s ⁻¹)
<i>K</i>	kinetic parameter
<i>q</i>	net radiation flux, Einstein (cm ⁻² s ⁻¹)
<i>R</i>	ideal gas constant (kJ mol ⁻¹ K ⁻¹)
<i>R</i>	reaction rate (M s ⁻¹)
<i>T</i>	absolute temperature (K)
<i>t</i>	time (s)
<i>V</i>	volume (m ³)
<i>X</i>	conversion
<i>x</i>	spatial coordinate (m)
<i>X_i</i>	coded variable

Greek letters

α	molar absorptivity (m ² mol ⁻¹)
Φ	primary quantum yield (mol Einstein ⁻¹)
κ	volumetric absorption coefficient (m ⁻¹)
Γ	reaction rate function defined in Eq. (4)
γ	dimensionless function defined in Eq. (2)
δ	dimensionless function defined in Eq. (2)
ξ	dimensionless function defined in Eq. (2)

Subscripts

<i>F</i>	relative to formic acid
<i>Fe²⁺</i>	relative to ferrous ion
<i>Fe³⁺</i>	relative to ferric ion
<i>L</i>	reactor depth
<i>P</i>	relative to hydrogen peroxide
<i>R</i>	relative to the photoreactor
<i>w</i>	wall property
λ	indicates a dependence on wavelength
∞	relative to the pre-exponential factor

Superscripts

<i>0</i>	initial condition
exp	experimental value
mod	model value
ref	reference value
<i>T</i>	thermal rate

Special symbols

$\langle \rangle$	average value
-------------------	---------------

Table 1

Reaction scheme for formic acid degradation.

Number	Reaction step	Constant
0	Fe(III) → Fe(II) + OH [•] + H ⁺	$\Phi_{\text{Fe(II),}\lambda}$
1	Fe(III) + H ₂ O ₂ → Fe(II) + H ⁺ + HO ₂ [•]	k_1
2	Fe(II) + H ₂ O ₂ → Fe(III) + OH ⁻ + HO [•]	k_2
3	H ₂ O ₂ + HO [•] → HO ₂ [•] + H ₂ O	k_3
4	Fe(II) + HO [•] → Fe(III) + OH ⁻	k_4
5	H ₂ O ₂ + HO ₂ [•] → HO [•] + HO ₂ [•] + O ₂	k_5
6	2HO [•] → H ₂ O ₂	k_6
7	2HO ₂ [•] → H ₂ O ₂ + O ₂	k_7
8	HO ₂ [•] + HO [•] → H ₂ O + O ₂	k_8
9	Fe(III) + HO ₂ [•] → Fe(II) + H ⁺ + O ₂	k_9
10	Fe(II) + HO ₂ [•] + H ⁺ → Fe(III) + H ₂ O ₂	k_{10}
11	HCOOH + HO [•] → CO ₂ ^{•-} + H ₂ O + H ⁺	k_{11}
12	CO ₂ ^{•-} + O ₂ + H ⁺ → CO ₂ ^{•-} + HO ₂ [•]	k_{12}
13	CO ₂ ^{•-} + Fe(III) → Fe(II) + CO ₂	k_{13}

organic compounds. The model describes the evolution of formic acid, hydrogen peroxide, and ferric ion concentrations in an isothermal, well-stirred tank photoreactor irradiated from the bottom. An experimental design based on the D-optimality criterion was adopted to avoid simultaneous high reaction temperatures and iron concentrations and, consequently, the precipitation of iron compounds. By applying a non-linear regression procedure, the Arrhenius kinetic parameters between 20 and 55 °C were estimated.

2. Kinetic model

The proposed kinetic model for the Fenton and photo-Fenton degradation of formic acid in aqueous solution is based on the reaction sequence reported by Walling and Goosen [1], Pignatello [17], and De Laat and Gallard [2]. The reaction scheme illustrated in Table 1 comprises 14 reaction steps, involving initiation, propagation, and termination reactions.

Formic acid, hydrogen peroxide, and ferrous ion degradation rate expressions are derived from the following assumptions: (i) the steady state approximation (SSA) may be applied for highly reactive radicals, such as OH[•], HO₂[•], and CO₂^{•-}, (ii) radical–radical termination reactions are neglected as compared with the propagation reactions, (iii) the oxygen concentration is always in excess, (iv) reaction of carbonyl radical with Fe(III) is neglected [24], and (v) reaction step 5 is neglected [4]. With these assumptions, the following reaction rates can be derived (see Appendix A):

$$\begin{bmatrix} R_F(x, t) \\ R_P(x, t) \\ R_{\text{Fe}^{2+}}(x, t) \end{bmatrix} = \begin{bmatrix} R_F^T(t) \\ R_P^T(t) \\ R_{\text{Fe}^{2+}}^T(t) \end{bmatrix} + \bar{\Phi}_{\text{Fe(II)}} \sum_{\lambda} e_{\lambda}^a(x, t) \begin{bmatrix} -\frac{1}{\delta} \\ \frac{1}{\delta} \left(1 - \frac{\gamma}{\xi}\right) \\ \frac{2\gamma}{\delta\xi} \end{bmatrix} \quad (1)$$

where

$$\gamma = K_3 \frac{C_P}{C_F} + 1; \quad \delta = \gamma + K_4 \frac{C_{\text{Fe}^{2+}}}{C_F}; \quad \xi = K_5 \frac{C_{\text{Fe}^{2+}}}{C_{\text{Fe}^{3+}}} + 1 \quad (2)$$

In Eqs. (1) and (2) $\bar{\Phi}_{\text{Fe(II)}}$ is the wavelength averaged primary quantum yield, $e_{\lambda}^a(x, t)$ is the spectral local volumetric rate of photon absorption (LVRPA), K_i are kinetic parameters, and C_F , C_P , $C_{\text{Fe}^{2+}}$, and $C_{\text{Fe}^{3+}}$ are the formic acid, hydrogen peroxide, ferrous ion, and ferric ion concentrations, respectively. The ferric ion concentration as a function of time, can be calculated from the initial ferric ion concentration ($C_{\text{Fe}^{3+}}^0$) and the actual ferrous ion concentration ($C_{\text{Fe}^{2+}}$):

$$C_{\text{Fe}^{3+}} = C_{\text{Fe}^{3+}}^0 - C_{\text{Fe}^{2+}} \quad (3)$$

iron concentrations of 9 ppm should be prevented to avoid the precipitation of ferric hydroxide [23] and, consequently, the subsequent reduction of the photo-Fenton efficiency.

In this paper, the kinetic modelling of the Fenton and photo-Fenton degradation rates employing formic acid as a model pollutant, for relatively low iron concentrations, is proposed. Formic acid is a by-product of the degradation of many hazardous

It should be noted that Eq. (1) for the three reacting species can be written by using the following matrix representation:

$$\mathbf{R}(x, t) = \mathbf{R}^T(x, t) + \bar{\Phi}_{\text{Fe(II)}} \sum_{\lambda} e_{\lambda}^a(x, t) \mathbf{\Gamma}(t) \quad (4)$$

The mathematical expression of the thermal reaction rate (first term on the right hand side of Eqs. (1) or (4)), may be represented by the expression

$$\begin{bmatrix} R_F^T(t) \\ R_P^T(t) \\ R_{\text{Fe}^{2+}}^T(t) \end{bmatrix} = -C_P \left\{ \frac{K_2 C_{\text{Fe}^{2+}}}{\delta} \begin{bmatrix} \delta - 1 + \frac{\gamma}{\xi} \\ 2 \left(\delta - \frac{\gamma}{\xi} \right) \end{bmatrix} + \frac{K_1 C_{\text{Fe}^{3+}}}{\xi} \begin{bmatrix} 0 \\ 1 \\ -2 \end{bmatrix} \right\} \quad (5)$$

In Eqs. (2) and (5), the following kinetic parameters have been defined

$$K_1 = k_1; \quad K_2 = k_2; \quad K_3 = \frac{k_3}{k_{11}}; \\ K_4 = \frac{k_4}{k_{11}}; \quad K_5 = \frac{k_{10}}{k_9} \quad (6)$$

Changes in the kinetic parameters with temperature have been correlated by the Arrhenius equation

$$\mathbf{K} = \mathbf{K}_{\infty} \exp\left(-\frac{\mathbf{E}}{RT}\right) \quad (7)$$

where \mathbf{K}_{∞} represents the array of pre-exponential factors, \mathbf{E} the array of activation energies, R the ideal gas constant, and T the absolute temperature.

3. Reactor model

3.1. Mass balances

The adopted experimental device is an isothermal, well-stirred tank photoreactor irradiated from the bottom [15]. The mass balance and the initial conditions for the formic acid, the hydrogen peroxide, and the ferrous iron, are given by the following set of first order, ordinary differential equations

$$\frac{d\mathbf{C}(t)}{dt} = \mathbf{R}^T(x, t) + \bar{\Phi}_{\text{Fe(II)}} \left\langle \sum_{\lambda} e_{\lambda}^a(x, t) \right\rangle_{V_R} \mathbf{\Gamma}(t) \quad (8)$$

$$\mathbf{C} = \mathbf{C}^0 \quad t = 0 \quad (9)$$

The required reaction rate expressions to replace in the mass balance equations are given by Eqs. (1)–(6).

3.2. Volumetric rate of photon absorption

To complete the theoretical description of the proposed kinetic model, it is necessary to introduce the expression of the spectral LVRPA on the right hand side of Eq. (1) or (4). Note that the radiation variable $e_{\lambda}^a(x, t)$ is a function of position and time.

Using a similar photoreactor, Alfano et al. [25] have proposed and verified experimentally a 3D radiation model to compute the spatial distribution of the absorbed photons inside the reactor. They found that, for restricted optical and geometrical parameters, changes in the radial and angular coordinates did not introduce significant variations on the radiation field. Accordingly, a 1D radiation field model has been used in this work to compute the spectral LVRPA. Thus:

$$e_{\lambda}^a(x, t) = \kappa_{\lambda}(t) q_w f_{\lambda} \exp[-\kappa_{T,\lambda}(t) x] \quad (10)$$

Here x is the spatial coordinate, t the reaction time, q_w the spectral net radiation flux at the reactor wall, f_{λ} the normalized spectral

distribution of the lamp output power, κ_{λ} the volumetric absorption coefficient of the reacting species, and $\kappa_{T,\lambda}$ the volumetric absorption coefficient of the reacting medium.

At the working pH 3.0, the iron complex $\text{Fe}(\text{OH})^{2+}$ is the dominant species [26]. Besides, for wavelengths greater than 300 nm, radiation absorption by hydrogen peroxide and ferrous iron is negligible. Consequently

$$\kappa_{T,\lambda}(t) \cong \alpha_{\text{Fe}(\text{OH})^{2+},\lambda} C_{\text{Fe}(\text{OH})^{2+}}(t) \quad (11)$$

For polychromatic radiation, an integration over the wavelength range of interest must be performed, accounting for the overlapping wavelength regions of lamp emission, reactor wall transmission and species absorption coefficient

$$\int_{\lambda_{\min}}^{\lambda_{\max}} e_{\lambda}^a(x, t) d\lambda \cong \sum_{\lambda_{\min}}^{\lambda_{\max}} e_{\lambda}^a(x, t) \quad (12)$$

Finally, the average volumetric rate of photon absorption inside the photoreactor should be evaluated and replaced on the right hand side of Eq. (8). Since the reactor cross-section is uniform, the reactor length average of the LVRPA must be calculated

$$\left\langle \sum_{\lambda} e_{\lambda}^a(x, t) \right\rangle_{V_R} = \frac{1}{x_L} q_w \sum_{\lambda} f_{\lambda} [1 - \exp(-\kappa_{\text{Fe}(\text{OH})^{2+},\lambda}(t) x_L)] \quad (13)$$

4. Experiments

4.1. Setup

Kinetic studies were performed in a well-stirred, batch, tank photoreactor. It was irradiated from the bottom with a black light, mercury arc lamp (Phillips TL K 40W/09N) placed at the focal axis of a cylindrical reflector of parabolic cross-section. The reactor was equipped with a liquid sampling valve, a variable-speed stirrer, a thermometer, and a shutter to isolate the reactor bottom from the emitting system. The experimental device was connected to a thermostatic bath to ensure isothermal conditions during the reaction time. More details on the stirred tank photoreactor can be found elsewhere [15].

4.2. Procedure

Reactant solutions of formic acid (Merck, ACS), hydrogen peroxide (Cicarelli, P.A.), and ferric sulphate (Carlo Erba, RPE) have been prepared. To avoid the precipitation of Fe(III), a stock solution of ferric sulphate was prepared and adjusted to pH \approx 1 with sulphuric acid.

Experimental runs began when solutions of ferric sulphate and formic acid were added to the reactor with distilled water at ambient temperature, and a concentrated sulphuric acid was used to adjust the pH to 3. Then, the temperature of the thermostatic bath was fixed at the specified working condition, the hydrogen peroxide solution added to the reactor, and the first sample withdrawn, defining the reaction time equal to zero. During the experimental run, the reaction temperature was kept constant and liquid samples were taken at equal time intervals.

For the irradiated experiments, the lamp was turned on with the shutter located between the lamp and the reactor window. Once the specified operating conditions were reached, the initial sample was taken and the lamp shutter removed to start the photo-Fenton experimental run.

As soon as the sample was withdrawn, Fenton reaction was stopped instantaneously by adding sodium sulphite. Formic acid was analyzed with total organic carbon measurements (Shimadzu

Table 2
Coded variables, operating conditions, and hydrogen peroxide and formic acid percent conversions ($t = 120$ min).

N	Coded variables				T (°C)	C _P /C _F	C _{Fe(III)} ⁰ (ppm)	Rad	X _P (%)	X _F (%)
	X ₁	X ₂	X ₃	X ₄						
1	-1	1	-1	-1	20	3	1	0	2.9	5.6
2	-1	1	-1	-1	20	3	1	0	1.4	3.8
3	-1	-1	-1	1	20	0.5	1	1	71.5	34.8
4	1	-1	-1	1	50	0.5	1	1	96.7	54.9
5	-1	-1	-1	-1	20	0.5	1	0	3.1	4.2
6	-1	-1	1	-1	20	0.5	9	0	16.3	5.4
7	1	-1	-0.125	-1	50	0.5	4.5	0	82.0	38.9
8	-1	1	-1	1	20	3	1	1	49.3	81.0
9	0.125	1	-1	1	36.9	3	1	1	85.3	98.0
10	1	1	-1	-1	50	3	1	0	64.7	96.2
11	-1	1	1	-1	20	3	9	0	17.1	26.8
12	-1	1	1	1	20	3	9	1	92.6	97.6
13	1	0	-1	-1	50	1.75	1	0	70.7	69.6
14	0.375	1	0.5	-1	40.6	3	7	0	75.1	93.5
15	1	1	-0.125	1	50	3	4.5	1	98.6	95.9
16	0	-1	-1	-1	35	0.5	1	0	19.9	6.2
17	-0.13	0	1	-1	33.1	1.75	9	0	59.8	70.5
18	-0.13	-1	1	1	33.1	0.5	9	1	98.2	43.1
19	-1	0.125	-0.125	1	20	1.9	4.5	0	8.6	15.7
20	-1	-1	0.125	1	20	0.5	5.5	1	94.3	51.2

TOC-5000A), hydrogen peroxide with a modified iodometric technique (UV-vis CARY 100 BIO, $\epsilon = 2.57 \times 10^4 \text{ M}^{-1} \text{ cm}^{-1}$ at 350 nm) [27], and ferrous ions with absorbance measurements of the Fe(II)-phenantroline complex ($\epsilon = 1.11 \times 10^4 \text{ M}^{-1} \text{ cm}^{-1}$ at 510 nm). Samples for total iron determination, were first treated with ascorbic acid and then analyzed by colorimetry with the 1,10-phenantroline method [28].

4.3. Design of experiments

The following working variables are considered for the experimental design method employed in this work: (i) reaction temperatures, T (°C) = [20; 55]; (ii) iron salt concentrations, $C_{\text{Fe}^{3+}}^0$ (ppm) = [1; 9]; (iii) hydrogen peroxide to formic acid initial concentration ratios, R = [0.5; 3] (corresponding to lower and higher amounts of hydrogen peroxide stoichiometric requirement), and (iv) two irradiation levels, Rad = [0; 1] (corresponding to dark or irradiated solution). These working variables are coded as X_1 , X_2 , X_3 , and X_4 , respectively.

As explained before, the precipitation of iron compounds during the experimental runs should be avoided. Accordingly, simultaneous high reaction temperatures and iron concentrations were prevented in the experimental design. For that reason, a D-optimal design was adopted. This method has been employed in those cases in which either any combination of values in the working variables is not possible (for instance, high temperatures and iron concentrations), or the number of experimental runs should be limited [29–31].

In order to generate the experimental design, it is necessary to define: (i) the grid on the experimental domain, (ii) the number of experiments, (iii) the order of the model, and (iv) the practical restrictions. The following grid and restrictions were selected:

$$X_i = \left[-1 : \frac{1}{16} : 1 \right], \quad (i = 1, 2, 3, \text{ and } 4) \quad (14)$$

$$X_1 + X_2 < 1 \quad \text{and} \quad X_4 = [1 - 1] \quad (15)$$

A quadratic model with interactions and a minimum number of experimental runs were also adopted.

Table 2 presents a summary of the coded variables and operating conditions for the experimental program. Hydrogen

peroxide and formic acid percent conversions after a reaction time $t = 120$ min are also reported in the last two columns.

5. Results

5.1. Regression of kinetic parameters

A non-linear, Newton Gauss–Marquardt optimization algorithm was applied to estimate the Arrhenius parameters involved in Eq. (7): the frequency (or pre-exponential) factor K_∞ and the activation energy E . The computed results of formic acid, hydrogen peroxide, and ferrous ion concentrations obtained with the kinetic model, were compared with the experimental concentrations obtained from samples at different reaction times. The optimization procedure provides the values of the Arrhenius parameters that minimize the differences between model predictions and experimental data.

The theoretical values were obtained solving the ordinary differential equation system Eqs. (8) and (9), using an algorithm for stiff problems. To compute the radiation field inside the photoreactor, the net radiative flux at the reactor bottom was evaluated with actinometric measurements employing potassium ferrioxalate in aqueous solution [32]; from these experiments, the following value was determined: $q_w = 1.59 \times 10^{-8} \text{ Einstein cm}^{-2} \text{ s}^{-1}$. The spectral data for the molar absorptivity of the absorbing species $[\text{Fe(III)OH}]^{2+}$ were obtained from Faust and Hoigné [26], the wavelength-averaged primary quantum yield ($\Phi_{\text{Fe(II)}} = 0.21$) was taken from Bossmann et al. [3], and the normalized spectral distribution of the lamp output power (f_λ) was provided by the lamp manufacturer.

Several authors have compared the traditional linear regression of the experimental results by applying the Arrhenius expression with the modern non-linear regression of these data [33–35]. Recently, Schwaab and Pinto [36] have suggested that, to preserve a statistic meaning of the correlation, a linear regression should be avoided. Thus, in this paper, the Arrhenius equation was introduced in the reaction rate expressions and all the parameters were estimated simultaneously by using the complete set of available experimental data.

It is also known that the high parameter correlation between K_∞ and E and the computational effort required for minimization of the objective function, can be diminished through the

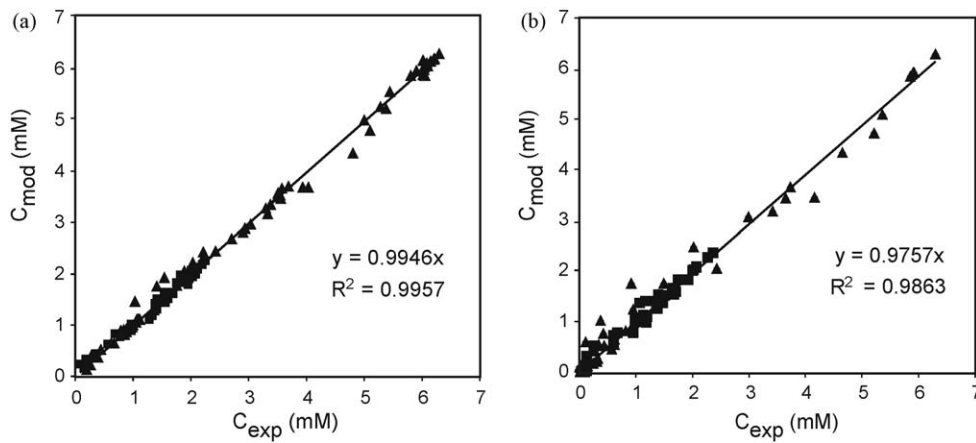


Fig. 1. Experimental vs. predicted concentrations. (a) Fenton. (b) photo-Fenton. Keys: (▲) hydrogen peroxide, (◆) Fe(II), (■) formic acid.

reparameterization of the Arrhenius equation, defining a reference reaction temperature. The following form of the Arrhenius equation has been suggested [36]:

$$K = K_{ref} \exp \left[\frac{E}{R} \left(\frac{1}{T_{ref}} - \frac{1}{T} \right) \right] \quad (16)$$

where K_{ref} is the kinetic constant at the reference temperature T_{ref} . A reference temperature equal to the average temperature of the analyzed experimental range has been defined in this work ($T_{ref} = 35 \text{ }^\circ\text{C}$).

From Eq. (16), the Arrhenius equation can be written as

$$K = \exp \left[A + B \left(\frac{T - T_{ref}}{T} \right) \right] \quad (17)$$

where the parameters of the reparameterized equation can be related to the parameters of the traditional Arrhenius equation by

$$A = \ln(K_{ref}) = \ln(K_\infty) - \frac{E}{RT_{ref}} \quad (18)$$

$$B = \frac{E}{RT_{ref}} \quad (19)$$

Values of the A_i and B_i estimated parameters and the corresponding traditional Arrhenius parameters $K_{\infty,i}$ and E_i , are shown in Table 3. The estimated values for the Arrhenius parameters E_3 , E_4 and E_5 obtained with the numerical procedure are insignificant [37], when they are compared with the values of E_1 and E_2 . Consequently, only

the activation energies for the kinetic parameters K_1 and K_2 are reported in the table.

Fig. 1 shows predicted and experimental concentrations for all the Fenton and photo-Fenton runs performed in the kinetic study. The symbols correspond to the formic acid, hydrogen peroxide, and ferrous ion concentrations obtained for different operating conditions and reaction times. Good agreement was found between simulation results and experimental data, with a root mean square error (RMSE) of 3.52% for the Fenton system and a RMSE of 11.76% for the photo-Fenton system. Considering $C_F > 0.10 \text{ mM}$ and $C_p > 0.08 \text{ mM}$, the RMSE for all the Fenton and photo-Fenton runs was 7.64%.

5.2. Formic acid degradation

Model predictions and experimental results of formic acid concentration as a function of the reaction time, for Fenton and photo-Fenton systems, were compared for different ferric iron concentrations, formic acid to hydrogen peroxide initial molar ratios, and reaction temperatures.

To study the effects produced on the pollutant degradation rates by addition of ferric iron, a set of experimental runs at constant values of the initial formic acid concentration ($2.0 \times 10^{-3} \text{ M}$) and the reaction temperature ($20 \text{ }^\circ\text{C}$) was performed. Fig. 2(a) shows model predictions and experimental data of the time evolution of formic acid relative concentration (C_F/C_F^0), for both the Fenton and photo-Fenton processes, for a constant

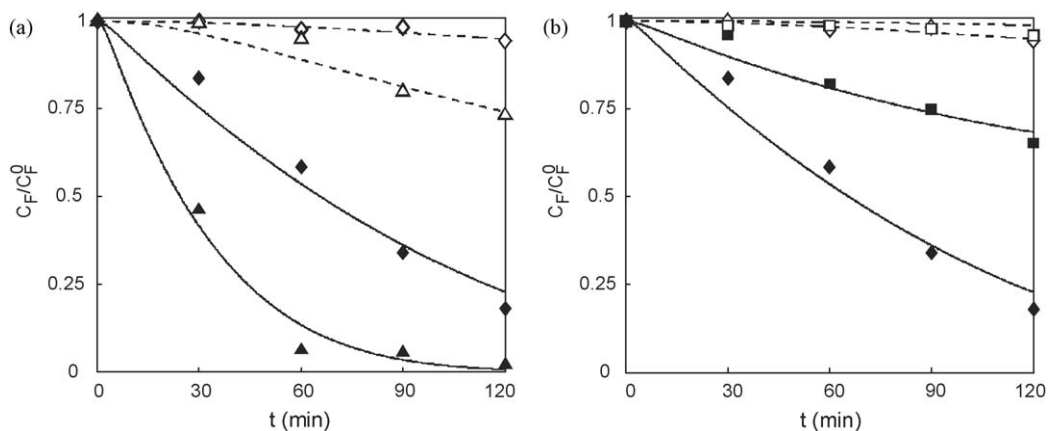


Fig. 2. Predicted and experimental relative concentrations of formic acid vs. time, for $C_F^0 = 2.0 \times 10^{-3} \text{ M}$ and $20 \text{ }^\circ\text{C}$. (a) $R = 3$, $C_{Fe(III)} = 1 \text{ ppm}$ (◇, ◆) and 9 ppm (△, ▲); (b) $C_{Fe(III)} = 1 \text{ ppm}$, $R = 0.5$ (□, ■) and 3 (◇, ◆). Keys: Fenton (---), photo-Fenton (—).

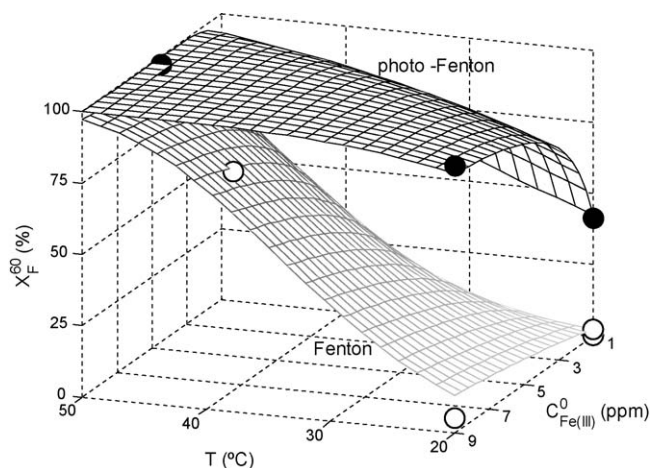


Fig. 3. Predicted and experimental formic acid conversions vs. reaction temperatures and ferric iron concentrations, for $t = 60$ min and $R = 3$. Keys for experimental results: Fenton (○), photo-Fenton (●).

value of the formic acid to hydrogen peroxide initial molar ratio ($R = 3$) and two ferric iron initial concentrations (1 and 9 ppm). Under the adopted operating conditions, it can be observed that: (i) the photo-Fenton system produces an organic pollutant conversion of 1300 and 265% greater than that obtained with the Fenton system for $C_{\text{Fe(III)}} = 1$ and 9 ppm, respectively, and (ii) an important increase in formic acid conversion is reached for the Fenton or the photo-Fenton process, when $C_{\text{Fe(III)}}$ is increased from 1 to 9 ppm.

Fig. 2(b) shows model predictions and experimental data of $C_{\text{F}}/C_{\text{F}}^0$ for dark and irradiated solutions, a constant concentration of the ferric iron (1 ppm), and two formic acid to hydrogen peroxide initial molar ratios ($R = 0.5$ and 3). Note that for $R = 0.5$, the amount of hydrogen peroxide is under the stoichiometric requirement ($R = 1$). As might be expected for this set of operating conditions, the formic acid conversion produced by the Fenton reaction is very low. In addition, due to the low ferric iron concentration employed in this study ($C_{\text{Fe(III)}} = 1$ ppm), an increase of R from 0.5 to 3 only yields an unimportant increment of the Fenton conversion. Conversely, even at these low concentrations of the iron salt, the photo-Fenton system produces moderate to high conversion levels: $X_{\text{F}} = 35\%$ for $R = 0.5$ and $X_{\text{F}} = 81\%$ for $R = 3$.

A 3D plot of formic acid conversions (after a reaction time $t = 60$ min), as a function of the reaction temperatures and of the ferric iron concentrations, is shown in Fig. 3. Predicted and experimental results for Fenton and photo-Fenton systems and for $R = 3$ are displayed. Notice that, for low and intermediate reaction temperatures, the photo-Fenton reaction always produces a formic acid conversion greater than that obtained with the Fenton system; for example, an experimental pollutant conversion enhancement of 265% is achieved for 20 °C and $C_{\text{Fe(III)}} = 9$ ppm. However, when the reaction temperature is increased, the pollutant conversion enhancement is reduced and, at the highest values of the reaction temperature, this conversion enhancement is almost undetectable.

Another important effect is observed when the ferric iron concentration is changed at low or intermediate reaction temperatures. One can observe that increasing the $C_{\text{Fe(III)}}$ increases the pollutant conversion and that when $C_{\text{Fe(III)}}$ is approximately equal to 9 ppm the conversion reaches a sort of plateau. On the other hand, at higher reaction temperatures, this effect of the $C_{\text{Fe(III)}}$ on the pollutant conversion is negligible.

These results indicate that the proposed kinetic model for Fenton and photo-Fenton degradation of formic acid, is capable of

Table 3

Estimated values of Arrhenius parameters.

Reparameterized parameters			Arrhenius parameters		
A_1	-4.60	± 0.15	$K_{\infty,1}$	1.38×10^{17}	$(\text{M}^{-1} \text{s}^{-1})$
A_2	3.12	± 0.23	$K_{\infty,2}$	1.92×10^9	$(\text{M}^{-1} \text{s}^{-1})$
A_3	-2.08	± 0.12	$K_{\infty,3}$	0.12	(-)
A_4	1.75	± 0.30	$K_{\infty,4}$	5.76	(-)
A_5	-3.35	± 0.70	$K_{\infty,5}$	0.035	(-)
B_1	44.07	± 3.87	E_1	112.87	(kJ mol^{-1})
B_2	18.26	± 1.85	E_2	46.76	(kJ mol^{-1})

predicting the experimental pollutant conversions with a good level of confidence.

6. Conclusions

The kinetic model for the Fenton and photo-Fenton degradation of a model pollutant (formic acid) in aqueous solution, as well as the corresponding procedures for the estimation of the Arrhenius kinetic parameters have been successfully validated. The reaction rate expression was developed considering an accepted reaction mechanism and accounting for the local volumetric rate of photon absorption inside the reactor.

To avoid the precipitation of iron compounds during the experimental runs, simultaneous high reaction temperatures and iron concentrations were prevented. To do this, an experimental design based on the D-optimality criterion was adopted.

The kinetic model was able to reproduce the combined effect of ferric iron concentrations, reaction temperatures, and formic acid to hydrogen peroxide initial molar ratios. Model predictions were compared with experimental data, and a good representation of the pollutant conversion was obtained. For all the investigated Fenton and photo-Fenton experimental runs, and considering formic acid concentrations greater than 0.10 mM and hydrogen peroxide concentrations greater than 0.08 mM, the maximum root mean square error was 7.64%. Therefore, the kinetic model obtained in this well-stirred tank laboratory reactor irradiated from the bottom can be used in a predictive way for scaling-up of a pilot plant solar reactor for the formic acid degradation.

Acknowledgments

The authors are grateful to Universidad Nacional del Litoral (UNL), Consejo Nacional de Investigaciones Científicas y Técnicas (CONICET) and Agencia Nacional de Promoción Científica y Tecnológica (ANPCyT). They also thank Tec. Antonio C. Negro for his valuable help during the experimental work.

Appendix A

Considering the assumptions (ii) to (iv) proposed in Section 2 for the kinetic model, the reaction rates for the n reacting species ($n = 7$) may be written by the following matrix representation:

$$\mathbf{R}(x, t) = \mathbf{S} \cdot \mathbf{K}'(x, t) \quad (\text{A.1})$$

Here $\mathbf{R}(x, t)$ is the array of reaction rates for the n reacting species, \mathbf{S} the stoichiometry matrix, and $\mathbf{K}'(x, t)$ the array of the reaction rates of each elementary step determined by the law of mass action. Eq. (A.1) for the stable species and free radicals may be also

represented by

$$R(x, t) = \begin{bmatrix} R_F(x, t) \\ R_P(x, t) \\ R_{Fe^{2+}}(x, t) \\ R_{Fe^{3+}}(x, t) \\ R_{OH\bullet}(x, t) \\ R_{CO_2\bullet-}(x, t) \\ R_{HO_2\bullet}(x, t) \end{bmatrix} = \begin{bmatrix} 0 & 0 & 0 & 0 & 0 & 0 & -1 & 0 & 0 \\ -1 & -1 & -1 & 0 & 0 & 1 & 0 & 0 & 0 \\ 1 & -1 & 0 & -1 & 1 & -1 & 0 & 0 & 1 \\ -1 & 1 & 0 & 1 & -1 & 1 & 0 & 0 & -1 \\ 0 & 1 & -1 & -1 & 0 & 0 & -1 & 0 & 1 \\ 0 & 0 & 0 & 0 & 0 & 0 & 1 & -1 & 0 \\ 1 & 0 & 1 & 0 & -1 & -1 & 0 & 1 & 0 \end{bmatrix} \cdot \begin{bmatrix} k_1 C_F C_P \\ k_2 C_{Fe^{2+}} C_P \\ k_3 C_{OH\bullet} C_P \\ k_4 C_{OH\bullet} C_{Fe^{2+}} \\ k_9 C_{HO_2\bullet} C_{Fe^{3+}} \\ k_{10} C_{HO_2\bullet} C_{Fe^{2+}} \\ k_{11} C_{OH\bullet} C_F \\ k_{12} C_{CO_2\bullet-} \\ \bar{\Phi}_{Fe(II)} \sum_{\lambda} e_{\lambda}^a(x, t) \end{bmatrix} \quad (A.2)$$

If the steady state approximation is applied to the free radicals OH•, HO₂•, and CO₂•⁻, the following expressions may be obtained

$$k_2 C_{Fe^{2+}} C_P - k_3 C_{OH\bullet} C_P - k_4 C_{OH\bullet} C_{Fe^{2+}} - k_{11} C_{OH\bullet} C_F + \bar{\Phi}_{Fe(II)} \sum_{\lambda} e_{\lambda}^a(x, t) = 0 \quad (A.3)$$

$$k_1 C_F C_P + k_3 C_{OH\bullet} C_P - k_9 C_{HO_2\bullet} C_{Fe^{3+}} - k_{10} C_{HO_2\bullet} C_{Fe^{2+}} + k_{12} C_{CO_2\bullet-} = 0 \quad (A.4)$$

$$k_{11} C_{OH\bullet} C_F - k_{12} C_{CO_2\bullet-} = 0 \quad (A.5)$$

Note that Eqs. (A.3)–(A.5) can be formally represented by a system of linear algebraic equations

$$\begin{bmatrix} -k_3 C_P - k_4 C_{Fe^{2+}} - k_{11} C_F & 0 & 0 \\ k_{11} C_F & k_{12} & 0 \\ k_3 C_P & k_{12} & -k_9 C_{Fe^{3+}} - k_{10} C_{Fe^{2+}} \end{bmatrix} \cdot \begin{bmatrix} C_{OH\bullet} \\ C_{CO_2\bullet-} \\ C_{HO_2\bullet} \end{bmatrix} = \begin{bmatrix} -k_2 C_{Fe^{2+}} C_P - \bar{\Phi}_{Fe(II)} \sum_{\lambda} e_{\lambda}^a(x, t) \\ 0 \\ -k_1 C_F C_P \end{bmatrix} \quad (A.6)$$

Using the definitions of δ , γ , and ξ (see Eq. (2) of the main body of the paper) and solving Eq. (A.6), one can write:

$$C_{OH\bullet} = \frac{k_2 C_{Fe^{2+}} C_P + \bar{\Phi}_{Fe(II)} \sum_{\lambda} e_{\lambda}^a(x, t)}{k_3 C_P + k_4 C_{Fe^{2+}} + k_{11} C_F} = \frac{k_2 C_{Fe^{2+}} C_P + \bar{\Phi}_{Fe(II)} \sum_{\lambda} e_{\lambda}^a(x, t)}{k_{11} C_F \delta} \quad (A.7)$$

$$C_{CO_2\bullet-} = \frac{k_2 C_F C_{OH\bullet}}{k_{12}} = \frac{k_2 C_{Fe^{2+}} C_P + \bar{\Phi}_{Fe(II)} \sum_{\lambda} e_{\lambda}^a(x, t)}{k_{12} \delta} \quad (A.8)$$

$$C_{HO_2\bullet} = \frac{k_1 C_{Fe^{3+}} C_P + (k_3 C_P + k_{11} C_F) C_{OH\bullet} - k_{12} C_{CO_2\bullet-}}{k_9 C_{Fe^{3+}} + k_{10} C_{Fe^{2+}}} = \frac{1}{k_9 C_{Fe^{3+}} \xi} \left(k_1 C_{Fe^{3+}} C_P + \gamma \frac{k_2 C_{Fe^{2+}} C_P + \bar{\Phi}_{Fe(II)} \sum_{\lambda} e_{\lambda}^a(x, t)}{\delta} \right) \quad (A.9)$$

Finally, Eq. (A.2) may be solved for $i = F, P, Fe^{2+}$. From the 3rd and 7th rows of the coefficient matrix **S**, it can be seen that $S_{Fe^{2+}j} = -S_{Fe^{3+}j}$. Accordingly, it is not necessary to solve Eq. (A.2) for $i = Fe^{3+}$.

For example, from Eqs. (A.2) and (A.7) and considering that $K_2 = k_2$ (see Eq. (6) of the paper), the final results for the formic acid ($i = F$) is:

$$R_F = (-1)k_{11} C_{OH\bullet} C_F = -\frac{k_2 C_{Fe^{2+}} C_P + \bar{\Phi}_{Fe(II)} \sum_{\lambda} e_{\lambda}^a(x, t)}{\delta} \quad (A.10)$$

$$R_F(x, t) = R_F^T(t) + \bar{\Phi}_{Fe(II)} \sum_{\lambda} e_{\lambda}^a(x, t) \left(-\frac{1}{\delta} \right) \quad (A.11)$$

$$R_F^T(t) = -C_P \left(\frac{K_2 C_{Fe^{2+}}}{\delta} \right) \quad (A.12)$$

The same procedure can be applied to get the reaction rate expressions for the remaining species: hydrogen peroxide ($i = P$) and ferrous ion ($i = Fe^{2+}$).

References

- [1] C. Walling, A. Goosen, J. Am. Chem. Soc. 95 (1973) 2987.
- [2] J. DeLaat, H. Gallard, Environ. Sci. Technol. 33 (1999) 2726.
- [3] S.H. Bossmann, E. Oliveros, S. Göb, S. Siegwart, E.P. Dahlen, L. Payawan, M. Straub Jr., M. Wörner, A.M. Braun, J. Phys. Chem. A 102 (1998) 5542.
- [4] J.J. Pignatello, E. Oliveros, A. MacKay, Crit. Rev. Environ. Sci. Technol. 36 (2006) 1.
- [5] G. Rupert, R. Bauer, J. Photochem. Photobiol. A: Chem. 73 (1993) 75.
- [6] O. Legrini, E. Oliveros, A.M. Braun, Chem. Rev. 93 (1993) 671.
- [7] H. Fallmann, T. Krutzler, R. Bauer, S. Malato, J. Blanco, Catal. Today 54 (1999) 309.
- [8] S. Chiron, A. Fernandez-Alba, A. Rodriguez, E. Garcia-Calvo, Water Res. 34 (2000) 366.
- [9] M. Rodriguez, V. Sarría, S. Esplugas, C. Pulgarin, J. Photochem. Photobiol. A: Chem. 151 (2002) 129.
- [10] C. Lee, J. Yoon, Chemosphere 26 (2004) 923.
- [11] J. Bacardit, A. Hultgren, V. Garcia-Molina, S. Esplugas, J. Adv. Oxid. Technol. 9 (2006) 27.
- [12] F. Torrades, M. Pérez, H.D. Mansilla, J. Peral, Chemosphere 53 (2003) 1211.
- [13] S. Malato, J. Blanco, M. Maldonado, P. Fernández, W. Gernjak, O. Alberola, Chemosphere 58 (2005) 391.
- [14] W. Gernjak, M. Fuerhacker, P. Fernández-Ibañez, J. Blanco, S. Malato, Appl. Catal. B: Environ. 64 (2006) 121.
- [15] J. Farias, G.H. Rossetti, E.D. Albizzati, O.M. Alfano, Ind. Eng. Chem. Res. 46 (2007) 7580.
- [16] G. Sagawe, A. Lehnard, M. Lübber, D. Bahnemann, Helv. Chim. Acta 84 (2001) 3742.
- [17] J.J. Pignatello, Environ. Sci. Technol. 26 (1992) 944.
- [18] Y. Sun, J.J. Pignatello, Environ. Sci. Technol. 27 (1993) 304.
- [19] G.H. Rossetti, E.D. Albizzati, O.M. Alfano, Sol. Energy 5 (2004) 443.
- [20] M. Pérez-Moya, M. Graells, L.J. del Valle, E. Centelles, H.D. Mansilla, Catal. Today 124 (2007) 163.
- [21] M. Lapertot, C. Pulgarin, P. Fernández-Ibañez, M.I. Maldonado, L. Pérez-Estrada, I. Oller, W. Gernjak, S. Malato, Water Res. 40 (2006) 1086.
- [22] J. García-Montaño, L. Pérez-Estrada, I. Oller, M. Maldonado, F. Torrades, J. Peral, J. Photochem. Photobiol. A: Chem. 195 (2008) 205.
- [23] R.S. Sapienszko, R.C. Patel, E. Matijevic, J. Phys. Chem. 81 (1977) 1061.
- [24] C.K. Duesterberg, W.J. Cooper, D. Waite, Environ. Sci. Technol. 39 (2005) 5052.
- [25] O.M. Alfano, R.L. Romero, A.E. Cassano, Chem. Eng. Sci. 40 (1985) 2119.
- [26] B.C. Faust, J. Hoigné, Atmos. Environ. 24A (1990) 79.
- [27] A.O. Allen, C.J. Hochanadel, J.A. Ghormley, J.A. Davis, J. Phys. Chem. 56 (1952) 575.
- [28] APHA, AWWA, WEF, Standard Methods for the Examination of Water and Wastewater, 19th ed., APHA, Washington, 1995, pp. 3–68.
- [29] B. Bourguignon, P.F. de Agular, M.S. Khots, D.L. Massart, Anal. Chem. 66 (1994) 893.
- [30] R. Carlson, Chemometr. Intell. Lab. Syst. 73 (2004) 151.
- [31] I. García, L. Sarabia, M.C. Ortiz, J.M. Aldama, J. Chromatogr. A 1085 (2005) 190.
- [32] H.J. Kuhn, S.E. Bravslavsky, R. Schmidt, Pure Appl. Chem. 76 (2004) 2105.
- [33] N. Brauner, M. Shacham, Chem. Eng. Process 36 (1997) 243.
- [34] R. Klicka, L. Kubacek, Chemometr. Intell. Lab. Syst. 39 (1997) 69.
- [35] R. Sundberg, Chemometr. Intell. Lab. Syst. 41 (1998) 249.
- [36] M. Schwaab, J.C. Pinto, Chem. Eng. Sci. 62 (2007) 2750.
- [37] Y. Lee, C. Lee, J. Yoon, Chemosphere 51 (2003) 963.